Dalton Transactions

PAPER

View Article Online
View Journal | View Issue

Cite this: *Dalton Trans.*, 2017, **46**, 12132

Mono-BHT heteroleptic magnesium complexes: synthesis, molecular structure and catalytic behavior in the ring-opening polymerization of cyclic esters†

I. E. Nifant'ev, *[a,b] A. V. Shlyakhtin,[a] V. V. Bagrov,[a] M. E. Minyaev,[b] A. V. Churakov,[c] S. G. Karchevsky,[d] K. P. Birin[e] and P. V. Ivchenko [a,b]

Numerous heteroleptic 2,6-di-*tert*-butyl-4-methylphenolate (BHT) magnesium complexes have been synthesized by treatment of (BHT)MgBu(THF)$_2$ with various alcohols. Molecular structures of the complexes have been determined by X-ray diffraction. The magnesium coordination number in [(BHT)Mg(μ-OBn)(THF)]$_2$ (**3**) and [(BHT)Mg(μ-O-*tert*-BuC$_6$H$_4$)(THF)]$_2$ (**4**) is equal to 4. Complexes formed from esters of glycolic and lactic acids, [(BHT)Mg(μ-OCH$_2$COOEt)(THF)]$_2$ (**5**) and [(BHT)Mg(μ-OCH(CH$_3$)COOCH$_2$COO^{t}Bu)(THF)]$_2$ (**6**) contain chelate fragments with pentacoordinated magnesium. Compounds **3–6** contain THF molecules coordinated to magnesium atoms. Complex {(BHT)Mg[μ-O(CH$_2$)$_3$CON(CH$_3$)$_2$]}$_2$ (**7**) does not demonstrate any tendency to form an adduct with THF. It has been experimentally determined that complexes **3** and **5** are highly active catalysts of lactide polymerization. The activity of **4** is rather low, and complex **7** demonstrates moderate productivity. According to DOSY NMR experiments, compounds **3** and **5** retain their dimeric structures even in THF. The free energies of model dimeric [(DBP)Mg(μ-OMe)(Sub)]$_2$ and monomeric (DBP)Mg(OMe)(Sub)$_2$ products on treatment of [(DBP)Mg(μ-OMe)(THF)]$_2$ with a series of σ-electron donors (Sub) have been estimated by DFT calculations. These results demonstrate that the substitution of THF by Sub in a dimeric molecule is an energetically allowed process, whereas the dissociation of dimers is energetically unfavorable. DFT modeling of ε-CL and (DL)-lactide ROP catalyzed by dimeric and monomeric complexes showed that a cooperative effect of two magnesium atoms occurs within the ROP for binuclear catalytic species. A comparison of the reaction profiles for ROP catalyzed by binuclear and mononuclear species allowed us to conclude that the binuclear mechanism is favorable in early stages of ROP initiated by dimers **3** and **5**.

Received 7th July 2017,
Accepted 28th August 2017

DOI: 10.1039/c7dt02469j

rsc.li/dalton

Introduction

Research and development of biodegradable and biocompatible polymers are of great interest from the perspective of designing new materials, which could reduce adverse environmental and health effects associated with their manufacture, use, and end-of-life properties.[1–10] Their applications span a wide field, ranging from green wrapping materials and fibres[11–13] to surgical polymers, tissue engineering, drug delivery and other biomedical applications.[5,14–18] The most frequently used biomedical polymers comprise homo- and copolymers of poly(lactic acid) (PLA), poly(glycolic acid) (PGA) and poly-(ε-caprolactone) (PCL).[19–24] Their synthesis *via* ring-opening polymerization (ROP) is most commonly conducted with tin(II) 2-ethylhexanoate Sn(Oct)$_2$.[25–28] Due to potential toxicity and unknown long-term effects of Sn^{2+} in tissues, the search for non-toxic and effective ROP catalysts for the purpose of biopolymer synthesis is of great interest.

[a]*M.V. Lomonosov Moscow State University, Department of Chemistry, Moscow, Russian Federation. E-mail: inif@org.chem.msu.ru, ilnif@yahoo.com*
[b]*A.V. Topchiev Institute of Petrochemical Synthesis, Russian Academy of Sciences, Moscow, Russian Federation*
[c]*N.S. Kurnakov Institute of General and Inorganic Chemistry, Russian Academy of Sciences, 31 Leninsky Prospect, 119991 Moscow, Russian Federation*
[d]*Institute of Petroleum Refining and Petrochemistry of the Republic of Bashkortostan, 12 Iniciativnaya Str., 450065 Ufa, Russian Federation*
[e]*A.N. Frumkin Institute of Physical Chemistry and Electrochemistry, Russian Academy of Sciences, 31 Leninsky Prospect, Building 4, 119071 Moscow, Russian Federation*

†Electronic supplementary information (ESI) available: Synthetic, X-ray and polymerization experimental details, NMR spectra, DFT calculations data. CCDC 1463808, 1545641–1545643, 1545645, 1545646, 1545648 and 1545650. For ESI and crystallographic data in CIF or other electronic format see DOI: 10.1039/c7dt02469j

Derivatives of "biometals", *i.e.*, Mg, Ca, Al and Zn, attract research attention due to their synthetic availability, low toxicity, and variable catalytic properties.[29–37]

Among "biometal" complexes, various magnesium alkoxides attract attention due to their high productivity[38,39] and facile synthesis from readily available organomagnesium compounds. The main problem in obtaining and using Mg-based ROP catalysts is the tendency of magnesium alkoxides to aggregate and form oligomeric and polymeric structures (Scheme 1).[40–43] Various types of chelating ligands are usually applied to prevent aggregation.[38,39,44–47] Alternatively, the aggregation can be prevented using bulky phenols as ligands at the magnesium atom (Scheme 1). 2,6-Di-*tert*-butyl-4-methylphenol (butylated hydroxytoluene, BHT) seems the most attractive phenol due to its availability. Bis-aryloxy complex $(BHT)_2Mg(THF)_2$ (**1**)[48] activated by alcohols was effectively used in the ROP of lactide,[49] ε-caprolactone[50] and ω-pentadecalactone.[51,52]

In our recent work,[53] we reported the synthesis, molecular structure and catalytic properties of the first well-defined dimeric heteroleptic BHT-alkoxy magnesium complex $[(BHT)Mg(\mu\text{-}OEt)(THF)]_2$ and compared its catalytic properties with those of the monomeric heteroleptic complex (BHT)Mg(OR)$(THF)_2$, which can be generated *in situ* by interaction of EtOH either with **1** or with $(BHT)MgBu(THF)_2$ (**2**) (Scheme 1). We determined that the catalytic properties of well-defined dimeric and generated monomeric species differ greatly. However, the chemical origin of this difference, the geometry of heteroleptic BHT-derived magnesium complexes and their tendency toward monomeric or dimeric structure formation remained unclear.

The present work is devoted to the synthesis of heteroleptic BHT-Mg-OR complexes containing various types of alkoxide ligands (RO) and to elucidation of their molecular structure in the solid state and in solution. Experimental study is complimented with evaluation of the thermodynamics of ligand exchange at the magnesium center and of the dissociation of dimeric complexes. Moreover, we performed comparative DFT modeling of ε-CL and DL-lactide ROP catalyzed by dimeric and monomeric BHT-Mg complexes. These results demonstrated the feasibility of both mechanisms of ROP of cyclic esters and allowed us to explain some of our experimental data.

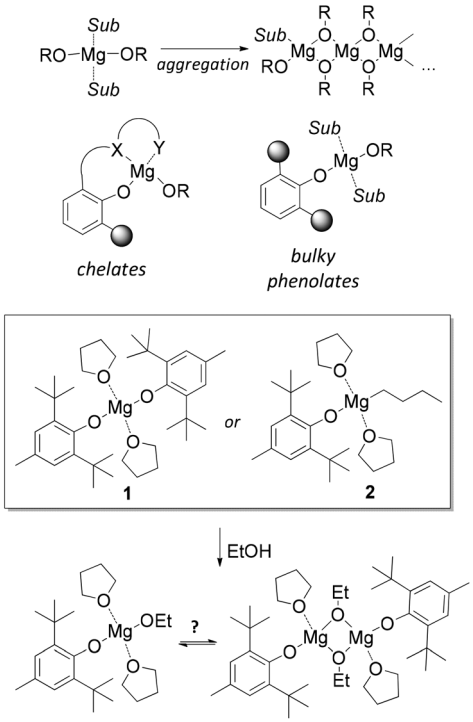

Scheme 1 Top: Magnesium alkoxide aggregation and prospective types of alkoxy-Mg catalysts. Middle and bottom: Monomeric and dimeric BHT-ethoxy magnesium complexes.

Experimental

$(BHT)_2Mg(THF)_2$ (**1**) was prepared using the modified method of Ittel.[48] $[(BHT)Mg(n\text{-}Bu)(THF)_2]$ (**2**) and $[(BHT)Mg(n\text{-}Bu)]_2$ were synthesized according to the literature procedure.[53]

Synthetic protocols and NMR spectra of BHT magnesium complexes **3–8** as well as polymerization experiment details are given in ESI.†

Corresponding CCDC numbers are 1463808, 1545641–1545643, 1545645, 1545646, 1545648, and 1545650† (for details see ESI†).

Results and discussion

Synthesis and solid state structures of BHT magnesium complexes

Earlier, we elaborated two alternative approaches to synthesize dimeric complex $[(BHT)Mg(\mu\text{-}OEt)(THF)]_2$ by using either reversible reaction between $(BHT)_2Mg(THF)_2$ (**1**) and EtOH (yield 66%) or an irreversible reaction of the heteroleptic aryloxy–alkyl complex $(BHT)Mg(n\text{-}Bu)(THF)_2$ (**2**) with ethanol (yield 94%).[53] In the present work, we have determined that a structurally analogous benzyloxy derivative, $[(BHT)Mg(\mu\text{-}OBn)(THF)]_2$ (**3**), can be obtained according to these two methods in yields of 82% and 92%, respectively (Scheme 2). Product **3**, obtained *via* reaction of **1** with BnOH, contained an admixture of benzyl alcohol and needed additional purification by recrystallization. Therefore to prepare compounds **4–7** we have used a method based on alcoholysis of the BHT-Mg-butyl complex **2** (Scheme 1). Complexes **4–7** were isolated in high yields as crystalline substances, which allowed us to study them by X-ray analysis.

The crystal structure of $[(BHT)Mg(\mu\text{-}OBn)(THF)]_2$ (**3**) contains two different isomers (Fig. 1, see ESI† for details) with a 1 : 1 ratio in the crystal lattice. In both dimeric molecules, the Mg atoms are in a distorted tetrahedral environment, possessing magnesium coordination number $CN_{Mg} = 4$. Two bridging benzyl groups connect two Mg atoms, forming a flat Mg_2O_2 rhomboid core. Both molecules exhibit the shortest distances

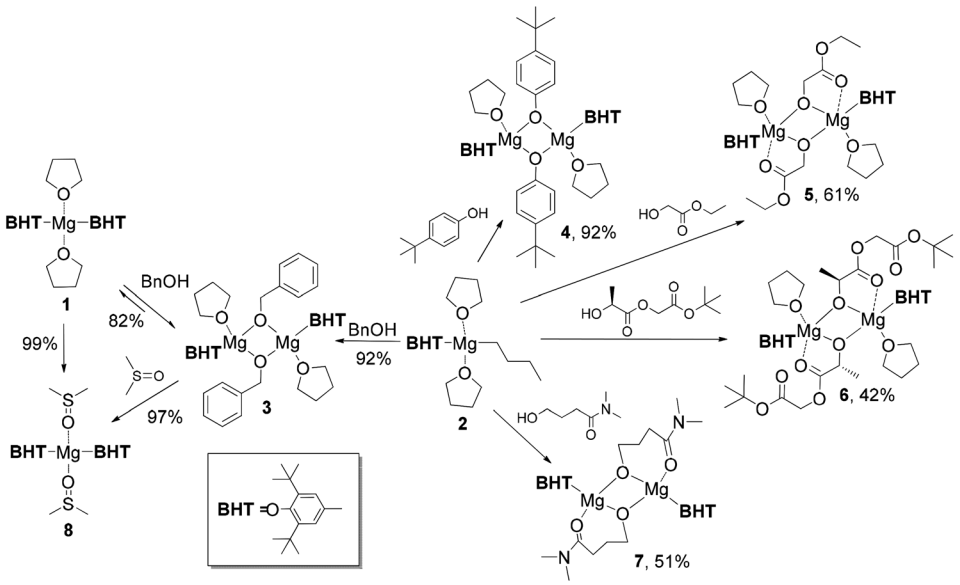

Scheme 2 Preparation and transformations of BHT-Mg complexes.

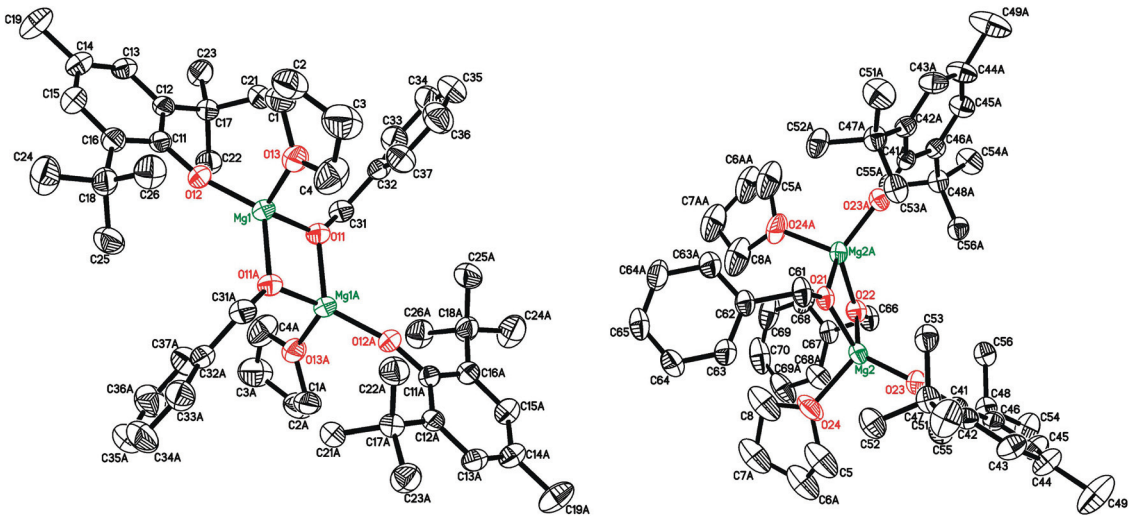

Fig. 1 Two independent molecules of [(BHT)Mg(μ-OBn)(THF)]$_2$ (**3**) with BHT (or THF) ligands being in *trans*- (left) and *cis*- (right) positions about the Mg_2O_2 core. Symmetry codes to generate equivalent atoms: $-x + 1, -y + 1, -z + 2$ for the left molecule; $x, -y + 3/2, z$ for the right molecule.

for Mg–O_{BHT} bonds, and the longest for Mg–O_{THF} (see ESI†). The *trans*-conformer **3** (Fig. 1, left) is structurally similar to previously published [(BHT)Mg(μ-OEt)(THF)]$_2$ [53] and dimeric BHT-guanidine complexes.[54]

Bis(aryloxy) magnesium heteroleptic complex [(BHT)Mg(μ-$OC_6H_4{}^{tert}$Bu)(THF)]$_2$ (**4**) was obtained in 92% yield *via* reaction of **2** with 4-*tert*-butylphenol in the presence of THF (Scheme 2). The molecular structures of **4** (Fig. 2, left) and the symmetric bis-aryloxy-complex (BHT)$_2$Mg(THF)$_2$ (**1**) (Fig. 2, right) were determined by X-ray diffraction. For both complexes CN_{Mg} = 4. The X-ray data for the closest analogue of **1**, (DBP)$_2$Mg(THF)$_2$ (DBP is the 2,6-di-*tert*-butylphenoxide anion), have been published.[55] The key structural parameters of complex **1** and (DBP)$_2$Mg(THF)$_2$ are nearly identical.

Unlike [(ArO)Mg(μ-ArO)]$_2$ (ArO = BHT, DBP), which form mononuclear complexes [(ArO)$_2$Mg(THF)$_2$] upon solvation with THF,[48] less sterically hindered [(BHT)Mg(μ-$OC_6H_4{}^{tert}$Bu)(THF)]$_2$ (**4**, Fig. 2) has a flat Mg_2O_2 rhomboid core (for details see ESI†) and does not display any tendencies toward monomer formation even in the presence of THF. The molecule is similar to *trans*-[(BHT)Mg(μ-OBn)(THF)]$_2$ (**3**, Fig. 1, left) described above.

The reaction of **2** with ethyl glycolate, HO-CH_2COOEt, yielded a dimeric complex [(BHT)Mg(μ-OCH_2COOEt)(THF)]$_2$ (**5**,

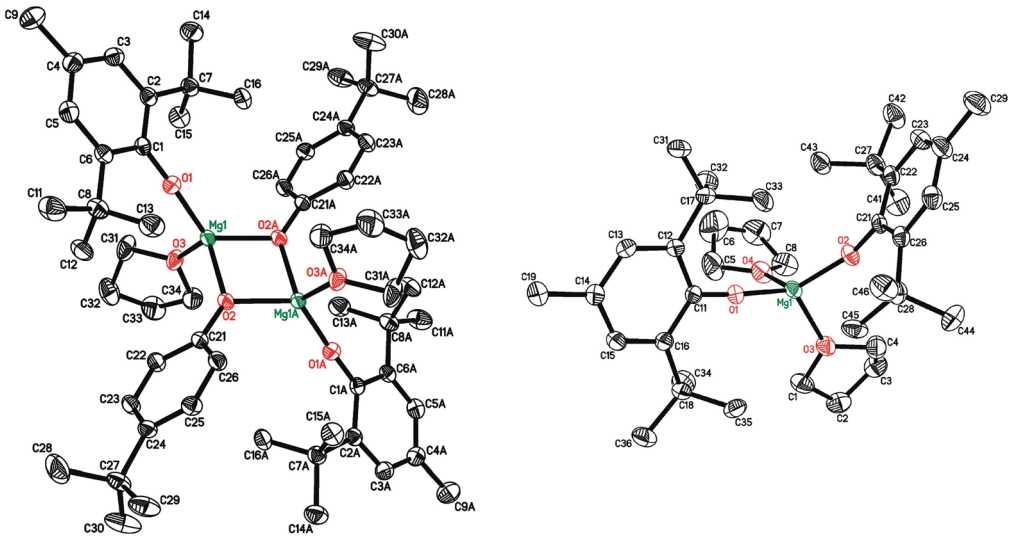

Fig. 2 Molecular structures of [(BHT)Mg(μ-$OC_6H_4{}^{tert}Bu$)(THF)]$_2$ (**4**, left) and $(BHT)_2Mg(THF)_2$ (**1**, right).

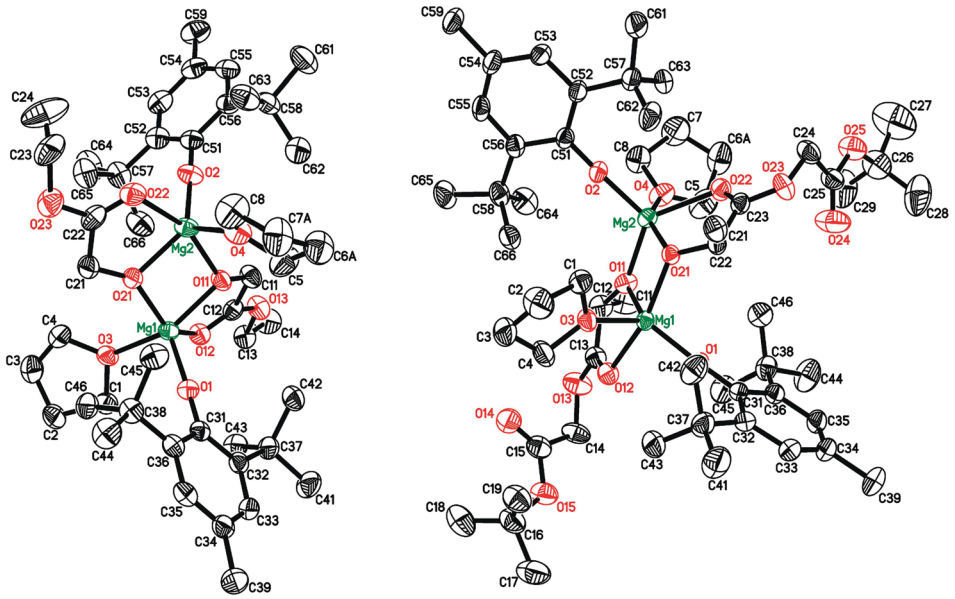

Fig. 3 Molecular structures of [(BHT)Mg(μ-OCH_2COOEt)(THF)]$_2$ (**5**, left) and [(BHT)Mg(μ-$OCH(CH_3)COOCH_2COO^tBu$)(THF)]$_2$ (**6**, right).

Scheme 2). According to the X-ray data (Fig. 3, ESI†), complex **5** contains an ethyl glycolate fragment in the μ–κ^1O:κ^2O,O′-semi-bridging coordination mode: the oxygen atom of the hydroxy group is bound to both Mg atoms, whereas the O-atom of the carboxy group is coordinated to only one of the magnesium atoms, making CN_{Mg} = 5. To the best of our knowledge, **5** is the first example of an aryloxy-glycolate magnesium complex characterized by X-ray diffraction.

The structure of the complex formed by the reaction of **2** with HO-CH_2COOEt depends on the reaction conditions. The slow diffusion of THF solutions of **2** and $HOCH_2COOEt$ yielded crystals of $[Mg_6(BHT)_2(OCH_2COOEt)_{10}](THF)_3$ possessing an unusual Mg_6O_{10} tetracubic core. The yield of this product was only 14%. However, due to poor crystal data, its crystal structure (see ESI†) was not deposited to the CSD.[56,57]

During lactide polymerization, various coordination modes of the growing polymeric chain to the metal atom are possible. Formation of such chelates is critically important for understanding the mechanism of coordination catalysis for the ROP of lactides.[58] The molecular structure of glycolate and lactate complexes of Al,[59–64] Mg,[65] Ga,[66] Y,[67] and Zn[68] have been determined for the "X-ray modeling" of the lactide polymerization mechanism. As it has been earlier determined by X-ray diffraction analysis for Al complexes, the μ–κ^1:κ^2 coordination type of the O-CHMeC(O)OCHMeCOOR fragment with a formation of five-membered chelates is observed in lactide ring-

opening products.[61,64] To determine the coordination mode in lactide polymerization by BHT-Mg complexes, we have synthesized in 42% yield crystalline dimer **6** (Scheme 2) – a product of the interaction of **2** with (*RS*) HO-CHMeCOOCH$_2$COO^{t}Bu. The structure of **6** (Fig. 3) shows that the preferable product is a five-membered chelate fragment with coordination of the closest carbonyl group to the magnesium atom. Compounds **5** and **6** have two non-coordinating solvent molecules in crystal channels. The non-coordinating molecules in crystals of **5** are highly disordered, therefore they have been deleted from the crystallographic model by the SQUEEZE method. ^{1}H and ^{13}C{^{1}H} NMR studies have confirmed that these molecules are THF and hexane in a 1 : 1 ratio.

The CN$_{Mg}$ in chelate heteroleptic complexes apparently depends on the geometry and the donor properties of the RO ligand. We reacted **2** with *N*,*N*-dimethyl-γ-hydroxybutyramide in a non-coordinating solvent (toluene) and in the presence of THF. Dimeric crystalline products [(BHT)Mg(μ-OCH$_2$CH$_2$CH$_2$CONMe$_2$)]$_2$ (**7**) and [(BHT)Mg(μ-OCH$_2$CH$_2$CH$_2$CONMe$_2$)]$_2$(THF)$_3$ (**7′**) were isolated from the reaction mixtures (Scheme 2). We studied both complexes by X-ray diffraction and determined that molecule **7** has a μ–κ^{1}O:κ^{2}O,O′ semibridging ligand coordination mode (Fig. 4) similar to that of **5** and **6**. Surprisingly, complex **7′** (for the ORTEP drawing see ESI†), synthesized in the presence of THF, does not contain coordinated solvent molecules, and CN$_{Mg}$ = 4. Conformations of {(BHT)Mg[O(CH$_2$)$_3$CON(CH$_3$)$_2$]}$_2$, in **7** and **7′** are nearly identical. Non-coordinating THF molecules in complex **7′** are in the outer sphere, filling the crystal channels. The various modes of coordination in dimeric complexes formed by glycolate/lactate and γ-hydroxybutyroylamide can be explained by steric factors (a longer γ-butyroyloxy fragment hinders THF coordination) and by the higher Lewis base strength of amides in comparison with esters. Typically, the Gutmann donor numbers for amides are double the donor numbers of ketones and esters.[69] An argument in favor of a higher donor ability of the oxygen-coordinated amide fragment is that the Mg–O$_{C=O}$ bonds are noticeably shorter in **7** and **7′** in comparison to those in **5** or **6**.

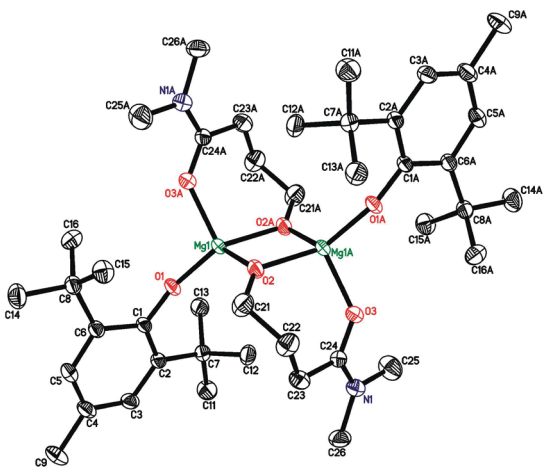

Fig. 4 Molecular structures of {(BHT)Mg[μ-O(CH$_2$)$_3$CON(CH$_3$)$_2$]}$_2$ (**7**). Symmetry code (A) to generate equivalent atoms: –*x*, –*y* + 1, –*z* + 1.

During synthesis of complexes **3**–**7** we used THF as a donor solvent. Considering the importance of the reaction media when using BHT complexes in coordination catalysis, we studied the interaction of donor solvents and dimeric complex **3**. In the reaction of **3** with DMSO, we observed a disproportionation with a formation of (BHT)$_2$Mg(DMSO)$_2$ (**8**), and the latter was isolated by crystallization in 97% yield based on BHT. This product is also formed in quantitative yield by the reaction of **1** with 2 eq. DMSO. We determined the structure of **8** by X-ray diffraction and found that despite significant differences in the donor properties of THF and DMSO, the basic geometric parameters of **1** and **8** are very close (for details, see ESI†).

Several observations and conclusions can be made regarding the results of experiments on the synthesis of BHT-derived magnesium complexes and their structural investigation. First, the stability of dimeric heteroletpic complexes depends on the Mg environment, such as BHT and RO ligands. The bridging position between Mg atoms is more efficiently taken up by relatively unhindered RO fragments, which is illustrated by the dimeric structure of the sterically less hindered phenolate [(BHT)Mg(μ-OC$_6$H$_4$^{tert}Bu)(THF)]$_2$ (**4**) in comparison to the monomeric structure of complex (BHT)$_2$Mg(THF)$_2$ (**1**) containing bulky phenolates only. Second, we suppose that the THF molecule mimics a coordinated cyclic ester molecule at the catalytic site within ROP. Therefore, one can conclude that the complexes with coordinated THF could be effective catalysts of ROP and conversely, complexes that cannot coordinate THF should be less active in ROP, especially in the beginning of the process. We see from the X-ray data that complexes **3** and **5** have THF coordinated to the Mg center, whereas complex **7** does not have this even though it possesses THF molecules in the crystal channels! Thus, we suppose that **7** should be less active than **3** and **5** at least at the beginning of the process. The catalytic activity of aryloxy-complex **4**, which contains coordinated THF molecules, depends on whether the aryloxy-group can initiate ROP. It has been shown that Mg phenolates can only initiate ROP of lactide at high temperatures (100–140 °C),[70] therefore, one can expect a modest initiation activity in ROP for complex **4** under mild conditions. Third, the magnesium coordination number in the "normal" alcoholates (**3**, **4**, **7**) is equal to 4, and CN$_{Mg}$ in glycolates (**5**, **6**) is equal to 5 due to chelate formation with the ester group of the glicolate. Assuming that the structure of **3** models the structure of the catalytic species of ROP of lactones, while the structures of **5** and **6** model the structure of the catalytic species of ROP of lactide, one can conclude that ROP of lactides and lactones should proceed *via* different mechanisms at least with dimeric BHT-magnesium catalysts.

Polymerization of ε-caprolactone and (DL)-lactide catalyzed by BHT-Mg complexes

In the current work, we started studying catalytic properties of heteroleptic BHT-Mg complexes with comparison of the catalytic behavior of monomeric complex (BHT)Mg(OBn)(THF)$_2$,

which can be generated *in situ* by interaction of BnOH with (BHT)MgBu(THF)$_2$ (**2**) (Scheme 1), and of its well-defined dimer [(BHT)Mg(μ-OBn)(THF)]$_2$ (**3**) in the ROP of ε-CL and (DL)-LA ([Mon]/[Cat] = 200, 25 °C, [monomer] = 1 M). We have found that polymerization of both ε-CL and (DL)-lactide proceeds faster, when a monomeric catalyst, generated from **2**/BnOH, is used, and is almost completed in 2 min under the given conditions (Table 1, runs 1 and 4). Dimeric catalyst **3** demonstrates slightly lower activity (Table 1, runs 2 and 5). In its presence, the reaction is almost completed in 10 min. It should be noted that catalysts **2**/BnOH and **3** outperform in catalytic activity widely known coordination catalysts such as tin(II) octanoate (typical reaction conditions: bulk, 120–180 °C temperature range) and aluminum(III) isopropoxide.[71,72]

To experimentally verify our suppositions regarding the influence of the structure of complex **3**, **4**, **5** and **7** on their catalytic properties, we studied (DL)-LA polymerization catalyzed by these precatalysts. The experiments were conducted at moderate monomer-catalyst ratios (75 : 1) to conclusively identify by NMR the fragments of the initiator –OR in PLA (Scheme 3) under mild conditions (20 °C). The results of polymerization experiments are summarized in Table 1. Assuming that the catalytic particles produced from **3**, **4**, **5** and **7** should be equal in activity (molecular structure of **6** indicates that there is no coordination between the Mg-center and the "second" ester fragment), the difference between the integral catalytic productivity of **3**, **4**, **5** and **7** depends strongly on the rate of the catalyst's formation within the initiation step

Table 1 ε-Caprolactone and (DL)-lactide polymerization catalyzed by complexes **2–5** and **7**. Reaction conditions: 20 °C, monomer concentration = 1 M in CH_2Cl_2

Run	Cat.	Mon.	[Mon]/[Cat]	React. time, min	Conv., %	$M_n \times 10^3$ (theor)[a]	$M_n \times 10^3$ (SEC)[b]	$Đ_M$	$M_n \times 10^3$ (NMR)[c]
1	**2**[d]	ε-CL	200	2	97	22.3	22.0	1.34	23.8
2	**3**	ε-CL	200	2	64	14.7	14.1	1.21	15.8
3	**3**	ε-CL	200	10	93	21.3	20.0	1.26	21.7
4	**2**[d]	*rac*-LA	200	2	95	27.5	25.6	1.41	27.8
5	**3**	*rac*-LA	200	2	76	22.0	20.8	1.37	22.2
6	**3**	*rac*-LA	200	10	94	27.2	25.4	1.38	26.9
7	**3**	*rac*-LA	75	2	96	10.4	11.1	1.33	10.9
8	**3**	*rac*-LA	75	10	>99	10.8	12.2	1.30	11.9
9	**5**	*rac*-LA	75	2	95	10.3	10.6	1.28	9.8
10	**5**	*rac*-LA	75	10	>99	10.8	10.9	1.24	10.1
11	**7**	*rac*-LA	75	2	65	7.0	—[e]	—[e]	11.5
12	**7**	*rac*-LA	75	10	98	10.6	16.4	1.38	15.9
13	**4**	*rac*-LA	75	10	18	1.9	—[e]	—[e]	—[e]
14	**4**	*rac*-LA	75	600	>99	10.8	29.4	1.54	30.7

[a] M_n (theor) = $MW_M \times [M]_0/[I]_0 \times$ conversion + MW_I, MW_M – molecular weights of monomers (114.14 for εCL, 144.13 for *rac*-LA), MW_I – molecular weight of initiator, $[M]_0/[I]_0$ – monomer to initiator initial concentration ratio. [b] Determined by SEC *vs.* polystyrene standards and corrected by a factors of 0.56 (εCL) and 0.58 (*rac*-LA). [c] Determined by the analysis of ^{1}H NMR spectra by the ratio of integral intensities of signals attributed to polymer OCH_2 (εCL) or CHMe (*rac*-LA) and initiator fragments. [d] Activated by 1 eq. of BnOH. [e] No data.

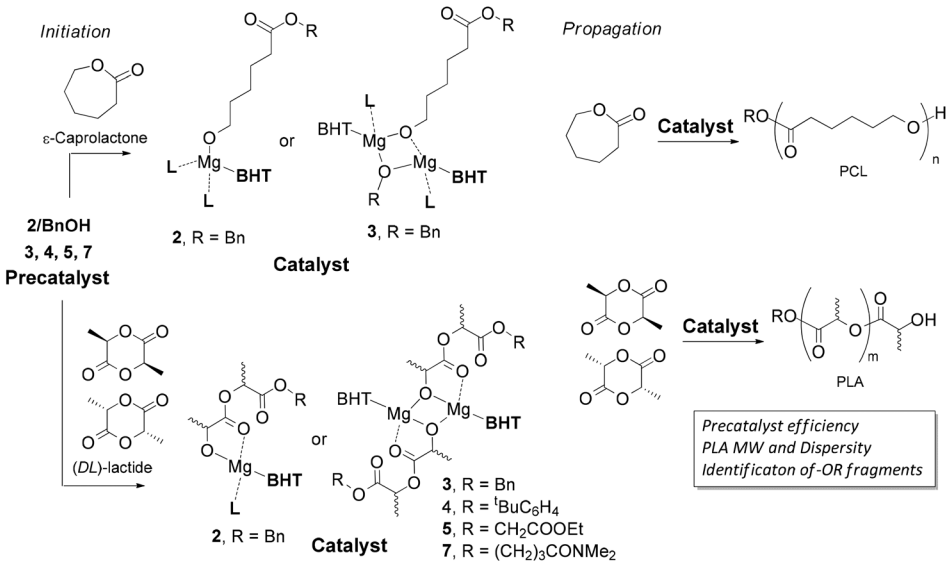

Scheme 3 Formation of PCL and PLA catalyzed by magnesium complexes **2–5** and **7**.

(Scheme 3). If the initiation rate for any of precatalysts **3**, **4**, **5** or **7** is lower than the propagation rate, one could expect that the M_n and $Đ_M$ values for PLAs would exceed their theoretical estimations.

We have found that complexes **3** and **5**, which contain THF coordinated to magnesium atoms, are effective catalysts of (DL)-lactide ROP (Table 1, runs 7–10). Monomer conversion for both catalysts after 2 minutes exceeded 90%. The full conversion was achieved in 10 minutes. The molecular weights of the polymers obtained by NMR (see ESI, Fig. S28–S36†) and SEC correspond to the theoretical values. Complex **7** demonstrated a significantly lower activity (Table 1, runs 11 and 12). Presumably, the relatively low activity of **7** is addressed by its modest predisposition to bind the monomer due to internal coordination of the Mg-center with the amide group of the pendant OR fragment. The difference between initiation and propagation rates leads to broadening of the molecular weight distribution of PLA and to a deviation between theoretical and experimental M_n values. This deviation becomes more significant in the case of aryloxy complex **4**, which has demonstrated extremely low initial catalytic activity. Upon hydrolysis after 10 minutes of the reaction, the ^{1}H NMR spectrum contained signals of 4-*tert*-butylphenol and BHT-H, products of decomposition of catalyst **4**, as well as (DL)-LA and PLA in a ratio of *ca.* 6 : 1 (see ESI, Fig. S35†). Almost full conversion was achieved after 10 hours. The molecular weight of PLA, which was obtained in the presence of **4**, is three times higher than M_n (theor). The product demonstrates a broader polydispersity (Table 2, run 14). Presumably, this is owing to lower nucleophilicity of the magnesium phenolate in comparison with magnesium alcoholates **3**, **5** and **7**. The rate of initiation by *tert*-butyl phenolate is an order of magnitude lower than the polymerization rate, so only a third of the molecules of **4** acts as catalytic particles. Therefore, the catalytic experiments confirmed in general our suppositions regarding the structure–activity relationship of BHT-Mg complexes.

Examination of the behavior of BHT-Mg complexes in solution

We have determined by X-ray diffraction that complexes [(BHT)Mg(OBn)(THF)]$_2$ (**3**) and [(BHT)Mg(OCH$_2$COOEt)(THF)]$_2$ (**5**) are dimers in the crystal with different CN_{Mg}. When discussing catalytic processes with **3** and **5** it is important to know whether the dimeric structure of these compounds is retained in solution, and in the presence of a large excess of electron-donating molecules, for example, THF. To experimentally verify whether complexes **3** and **5** are present in THF solution as monomers or dimers, we have used the method of diffusion-ordered NMR spectroscopy (DOSY NMR).[73]

It is known that for spherical molecules the diffusion coefficient (D) is related to molecule size *via* the Stokes–Einstein equation (eqn (1)),[74] where k is the Boltzmann constant, T – temperature, η – dynamic viscosity, R_S – hydrodynamic molecular radius. Methods of DOSY NMR allow evaluating the diffusion coefficient of the molecule and thus the molecular size of Mg-BHT derivatives according to eqn (1) and (2). The DOSY NMR spectrum is registered with coordinates chemical shift/lg D, which allows us to experimentally determine lg D and, consequently, gauge the R_S of BHT-Mg derivatives in solution (eqn (2)).

$$D = \frac{kT}{6\pi\eta R_S} \quad (1)$$

$$R_S = \frac{kT}{6\pi\eta} \cdot 10^{-\lg D} \quad (2)$$

The abovementioned equations refer to molecules of spherical shape. Nevertheless, they can be used for other types of molecules if the rotational rate exceeds the rate of progressive motion of the molecule. It can be gathered from eqn (2) that the observed R_S in the DOSY NMR experiment is inversely proportional to the dynamic viscosity of the specific BHT-Mg derivative solution being examined. This value depends on the viscosity of the solvent and on the concentration of the studied compound, and cannot always be predicted or measured with adequate accuracy for the concentrated solutions required to register DOSY NMR spectra of good quality. As a result, the observed accuracy of lg D for BHT-Mg derivative solutions is inadequate for accurately calculating R_S. Thus, the DOSY experiments we conducted under formally identical conditions for complex [(BHT)Mg(μ-OBn)(THF)]$_2$ in THF-d$_8$ gave lg D values from −9.086 to −9.191, which corresponds to a 27% error in R_S determined by eqn (2). To remove this uncertainty in calculating dynamic viscosity, we propose to use an internal

Table 2 $R_{S(dimer)}/R_{S(1)}$ and $R^W_{eq(dimer)}/R^W_{eq(1)}$ for dimeric complexes [(BHT)Mg(OBn)(THF)]$_2$ (**3**) and [(BHT)Mg(OCH$_2$COOEt)(THF)]$_2$ (**4**) relative to (BHT)$_2$Mg(THF)$_2$ (**1**); and calculated $R^W_{eq}/R^W_{eq(1)}$ for monomeric (BHT)Mg(OBn)(THF)$_2$ and (BHT)Mg(OCH$_2$COOEt)(THF)$_2$

	DOSY NMR		X-ray data		DFT calc.	
	Δlg D	$R_{S(dimer)}/R_{S(1)}$	R^W_{eq}	$R^W_{eq(dimer)}/R^W_{eq(1)}$	R^W_{eq}	$R^W_{eq}/R^W_{eq(1)}$
(BHT)$_2$Mg(THF)$_2$ (**1**)	—[a]	—	5.138	—	5.220	—
(BHT)Mg(OBn)(THF)$_2$	0.076	1.191	—	—	4.838	0.927
[(BHT)Mg(OBn)(THF)]$_2$ (**3**) (*trans*)			5.685	1.107	5.773	1.106
(BHT)Mg(OCH$_2$COOEt)(THF)$_2$	0.078	1.197	—	—	4.542	0.870
[(BHT)Mg(OCH$_2$COOEt)(THF)]$_2$ (**4**)			5.628	1.095	5.714	1.095

[a] No data.

standard,[73,75,76] which can be a chemically inert compound of similar nature and size. To study complexes **3** and **4**, we used $(BHT)_2Mg(THF)_2$ (**1**) as such a standard, possessing a monomeric structure in THF media.[48] According to this approach and eqn (2), the difference $\Delta\lg D = \lg D_{(1)} - \lg D_{(dimer)}$ is connected with the ratio of hydrodynamic radii $R_{S(dimer)}/R_{S(1)}$ by a simple equation that excludes such values as T and η, because the measurement of $\lg D_{(dimer)}$ and $\lg D_{(1)}$ occurs in the same experiment (eqn (3)),

$$\frac{R_{S(dimer)}}{R_{S(1)}} = \frac{c_{(1)} f_{s(1)}}{c_{(dimer)} f_{s(dimer)}} \cdot 10^{\Delta \lg D} \quad (3)$$

where $c_{(1)}$ and $c_{(dimer)}$ are size correlation factors between R_S and $R^W_{eq(solvent)}$, $f_{s(1)}$ and $f_{s(dimer)}$ are shape friction correction factors[77–80] for monomeric (**1**) and for dimeric (**3** and **4**) complexes (see ESI† for corresponding formulae for c and r factors). Because $R_{S(1)}$ can be determined based on X-ray diffraction data, it becomes possible to estimate $R_{S(dimer)}$ with sufficiently high accuracy. We recorded the DOSY NMR spectra of complexes $[(BHT)Mg(OBn)(THF)]_2$ (**3**) and $[(BHT)Mg(OCH_2COOEt)(THF)]_2$ (**5**) in the presence of $(BHT)_2Mg(THF)_2$ (**1**) (see ESI, Fig. S27†). Based on these spectra, we determined the values of $\Delta\lg D$ and the $R_{S(dimer)}/R_{S(1)}$ ratios (see Table 2).

We compared the obtained data with the R^W_{eq} values determined from the X-ray diffraction experiments for **1**, **3** and **5**, as well as from the DFT data for molecular structures of dimeric complexes **1**, **3**, **5** and hypothetical monomeric complexes $(BHT)Mg(OBn)(THF)_2$ and $(BHT)Mg(OCH_2COOEt)(THF)_2$ (see Table 2). The $R^W_{eq(dimer)}/R^W_{eq(1)}$ values for dimeric complexes **3** and **4** calculated and confirmed by X-ray diffraction are in good agreement with the experimental values, while the $R^W_{eq}/R^W_{eq(1)}$ ratios for calculated hypothetical monomeric structures $(BHT)Mg(OBn)(THF)_2$ and $(BHT)Mg(OCH_2COOEt)(THF)$ (0.927 and 0.870, respectively) correspond to the regions of the DOSY NMR spectrum where no signals are observed. Therefore, we can state that complexes **3** and **4** possess a dimeric structure in THF solution.

DFT modeling of ligand exchange and dissociation for dimeric BHT-Mg complexes

The tendency of heteroleptic BHT-magnesium complexes to form dimers is confirmed by the results of X-ray analysis of compounds **3–7**, as well as DOSY NMR spectra of complexes **3** and **5**. Complexes of formula $[(BHT)Mg(\mu\text{-}OR)(THF)]_2$ are precursors of ROP catalysts and can form two principally different types of catalytic particles under treatment with a molecule of cyclic ester (Scheme 4):

- *Binuclear* catalytic species are formed as a result of substitution of THF with a molecule of cyclic ester – an ROP substrate (Sub);

- *Mononuclear* catalytic species are formed during the dissociation of BHT-alkoxy dimers with parallel solvation with two Sub molecules.

We determined whether the thermodynamics are favorable for the formation of both types of catalytic particles. We calculated the free energy G°_{298} of the interaction of model compound $[(DBP)Mg(\mu\text{-}OMe)(THF)]_2$ (D_{THF}) with one and two equivalents of Sub (per mol of Mg) – monomers used in ROP and typical solvents (Scheme 4). The change in free energy during ligand exchange (per mol of Mg) ΔG_{LE} was calculated as the difference in free energies of $[(DBP)Mg(\mu\text{-}OMe)(Sub)]_2$ (D_{Sub}) and D_{THF} with the free energies of Sub and THF considered using the formula $\Delta G_{LE} = 1/2[G^{\circ}_{298}(D_{Sub}) - G^{\circ}_{298}(D_{THF}) - 2G^{\circ}_{298}(Sub) + 2G^{\circ}_{298}(THF)]$. The values of ΔG_{LE} (Table 3) characterize the relative ability of Sub to coordinate to the Mg atom in a dimeric DBP-methoxy complex. Coordination with the examined complexes is not sterically hindered, therefore, ΔG_{LE} can be viewed as a measure of ligand donor ability, an analogue of the Gutmann donor number, an experimentally determined characteristic of ligands and solvents (Table 3).[69,81] The comparison of ΔG_{LE} for various substrates Sub allows us to form a range of donor abilities (Scheme 4). As shown in Table 3, THF is in the middle of this range, therefore, its replacement with Sub during ROP in the presence of excess Sub is thermodynamically permissible.

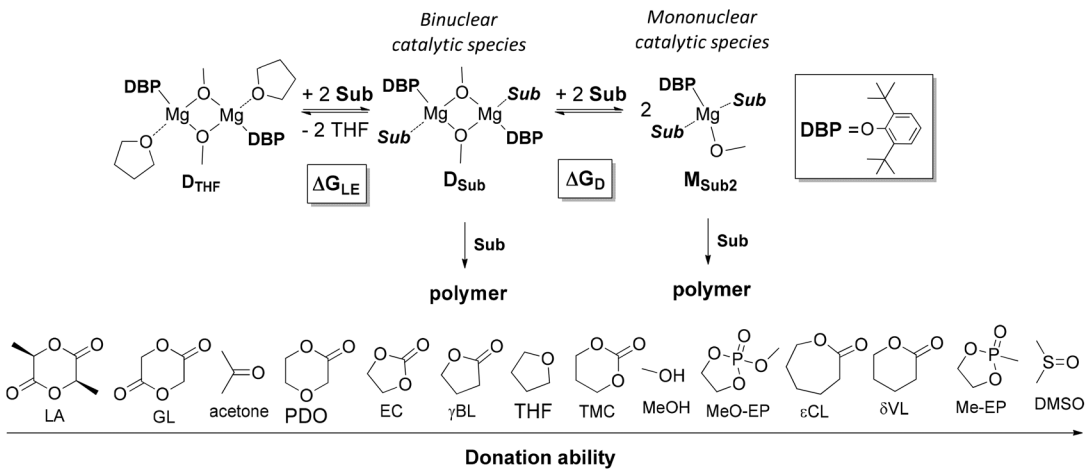

Scheme 4 Ligand exchange and dissociation of model DBP-methoxy complexes. Sub donation ability range.

Table 3 The change in free energy during formation (ΔG_{LE}) and dissociation (ΔG_D) of dimeric complexes [(DBP)Mg(μ-OMe)(Sub)]$_2$. The Gutmann donor numbers for some esters and solvents Sub[81]

S	ΔG_{LE}, kcal mol^{-1}	ΔG_D, kcal mol^{-1}	Donor number
LA	3.01	16.88	—[a]
GL	2.78	16.83	—
Acetone	1.38	14.90	17
PDO	0.90	15.24	—
EC	0.82	18.52	16.4
γBL	0.60	15.06	18
THF	0.00	17.99	20
TMC	−0.87	15.17	—
MeOH	−1.49	11.12	19
MeO-EP	−1.81	13.49	23[b]
εCL	−2.04	15.66	—
δVL	−2.06	15.30	—
Me-EP	−5.47	9.51	—
DMSO	−7.41	7.75	29.8

[a] No data. [b] For trimethyl phosphate.

Table 3 also contains the free energies ΔG_D of monomeric complex $\mathbf{M_{Sub2}}$ formation (Scheme 4). As a hypothetical structure of the monomeric complex we chose tetrahedral (DBP)Mg(μ-OMe)(Sub)$_2$, which is isostructural to (BHT)Mg(Bu)(THF)$_2$.[53] The calculation was made according to the formula $\Delta G_D = G^{\circ}_{298}(\mathbf{M}_{Sub2}) - 1/2G^{\circ}_{298}(D_{Sub}) - G^{\circ}_{298}(Sub)$. We found that the formation of monomeric complexes is energetically unfavorable for all solvating substrates ($\Delta G_D > 0$). The dissociation energy for all Sub except for DMSO and Me-EP is higher than 13 kcal mol^{-1}, which prevents this reaction under mild conditions.

DFT modeling of ROP catalyzed by monomeric and dimeric BHT-alkoxy magnesium species

Using X-ray diffraction analysis, DOSY NMR experiments and DFT calculations of ligand exchange and dissociation processes, we have determined that the dimeric structure for heteroleptic BHT-alkoxy magnesium complexes is more favorable in both the solid state and solution. During the next stage of our work we conducted a DFT study of the polymerization mechanism. For BHT-alkoxy-Mg complexes two principally different ROP mechanisms are possible: a traditional mononuclear coordination–insertion mechanism, which is realized if the dimeric complex is dissociated beforehand with formation of monomeric BHT-alkoxy catalyst species, and the alternative and novel binuclear ROP mechanism with direct involvement of dimeric bimetallic catalytic particles. To determine which mechanism is more favorable, we analyzed the reaction profiles of lactone and lactide polymerization for monomeric and dimeric catalyst species. εCL was chosen as the substrate during modeling of the lactone ROP reaction profile, whereas DL-lactide was used to model lactide ROP.

Polymerization of εCL

Mononuclear catalyst. There are several articles regarding DFT-modeling of lactone ROP initiated by mononuclear "biometal" alkoxides.[82–90] Moreover, only a few of them describe full reaction profiles including a set of key stationary points and transition states. Similar reaction profiles of εCL polymerization were drawn up for complexes of Al,[85–88] Ca[82] and Mg.[90] During the modeling of lactone ROP, metal methoxy-complexes are used as initial structures; the methoxy group adequately models the growing polymer chain in truncated models of ROP.[91–93]

Earlier, we determined by DFT calculations that BHT-Mg-OMe complexes containing one or three molecules of coordinated monomer (CN_{Mg} = 3 and 5, respectively), are significantly higher in energy than tetrahedral complexes.[90] In this work, we used the tetrahedral complex (DBP)Mg(OMe)(εCL)$_2$ as a model catalytic particle and starting stationary point on the mononuclear reaction profile, **I-1CL**. The calculations showed that during the first stage from **I-1CL**, through the transition state **TS-12CL**, a hemi-acetal complex **I-2CL** is formed. Then, the bond between Mg–OMe and the endocyclic oxygen atom coordinated to Mg is cleaved (*via* **TS-23CL**), which leads to formation of **I-3CL**. This reaction is followed by cleavage of the (O)C–O bond, which corresponds to the transition state **TS-34CL**. The concomitant dissociation of the M···O=C(OR)– in **I-4CL** can occur with the coordination of a second molecule of εCL. The process occurs *via* the low-energy "dispersed" **TS-45CL**, the exact geometry of which we could not determine (the relative energy of **TS-45CL** obtained by scanning the potential energy surface was 5–6 kcal mol^{-1}). The product **I-5CL** formed during the coordination of the second molecule of εCL is a structural analog of **I-1CL**. Stationary points **I-1CL**–**I-5CL** and transition states **TS-12CL**, **TS-23CL** and **TS-34CL** form the reaction profile of the single-center ROP of εCL (Fig. 5). The activation barrier of this reaction is 14.8 kcal mol^{-1}.

Binuclear catalyst. To the best of our knowledge, the binuclear mechanism of lactone ROP has never been studied with DFT. The calculated energy profile for the binuclear mechanism of εCL ROP is given in Fig. 5. We propose that the starting stationary point **DI-1CL** is a symmetric dimer [(DBP)Mg(μ-OMe)(εCL)]$_2$ structurally similar to complex **3**. The dimeric complex can contain one or two coordinated molecules of εCL. Calculations have shown that complex **DI-1CL′**, which contains one coordinated molecule of εCL, is only 3.5 kcal mol^{-1} higher in energy than **DI-1CL**. As opposed to **I-1CL** in the mononuclear mechanism, in **DI-1CL** and **DI-1CL′** the methoxy group that initiates ROP is bonded with two atoms of magnesium. The nucleophilic insertion of the methoxy group to the carbonyl group of the coordinated εCL requires the cleavage of one of the bonds of Mg–OMe, and we can expect a high activation energy for this process. On the other hand, binuclear catalysis, as opposed to the mononuclear process, displays a cooperative effect of the di-Mg core. In our case, this effect means that the insertion of –OMe is preceded by the formation of a stationary point with coordination of the endocyclic oxygen atom to the second Mg atom **DI-1cCL′** (Scheme 5).

This process requires only 1.3 kcal mol^{-1}, but the formation of **DI-1cCL′** obviously increases the Arrhenius pre-exponential factor for a binuclear mechanism. For **DI-1CL**, this type of

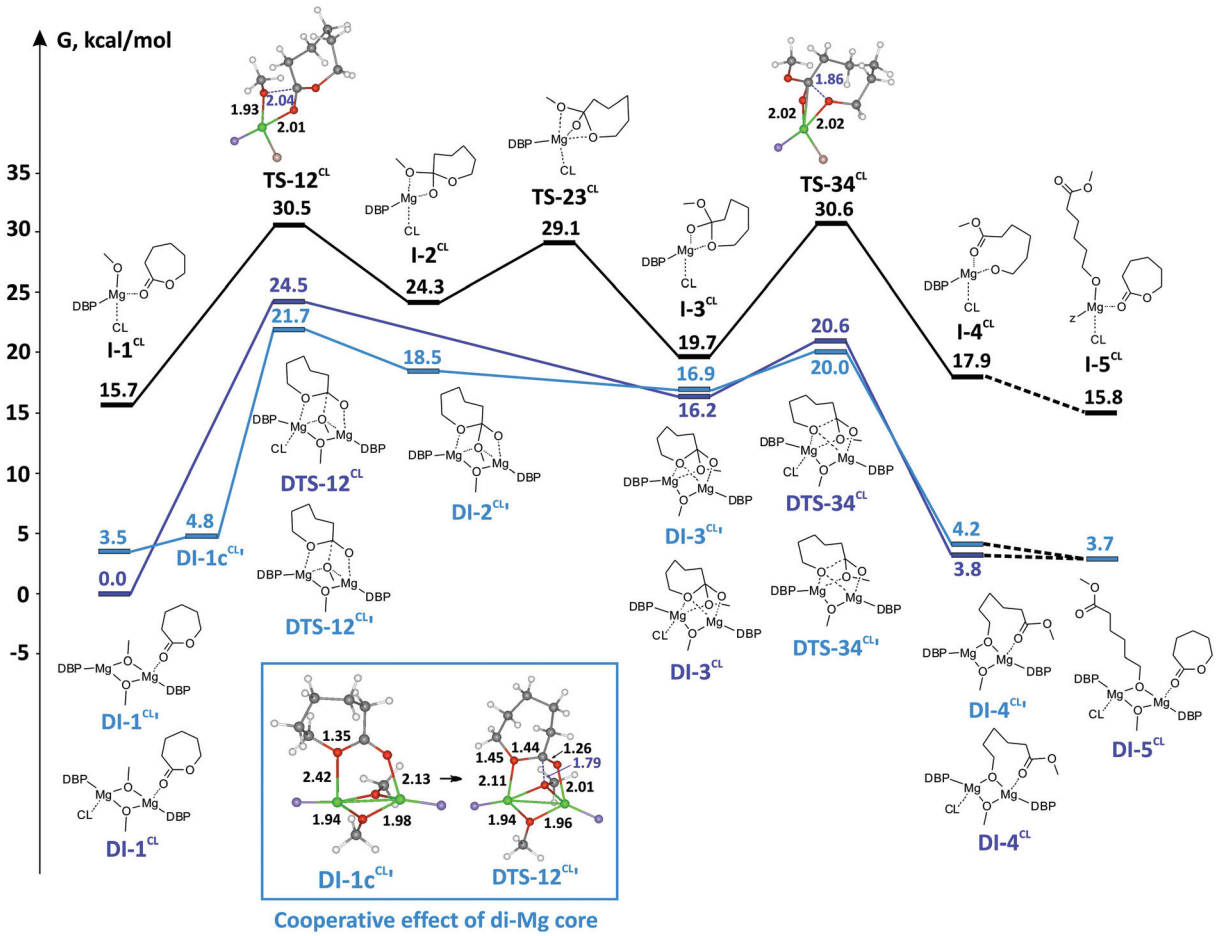

Fig. 5 Reaction profiles of εCL ROP for mononuclear and binuclear coordination–inserition mechanisms. DBP and second εCL fragments are omitted for clarity, phenolate and εCL oxygen atoms are colored in blue and pink, correspondingly.

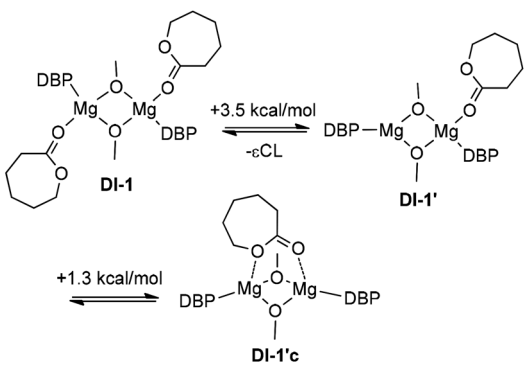

Scheme 5 Cooperative effect of the di-Mg core before –OMe insertion.

intermediate is not fixed. Therefore, we can assume that on the main reaction pathway **DI-1CL** loses one molecule of εCL, with the formation of **DI-1cCL′**. The energy of the first transition state **DTS-12CL′** between **DI-1cCL′** and **DI-2CL** is significantly (2.8 kcal mol^{-1}) lower than the energy of **DTS-12CL**. A possible reason for this is that in **DTS-12CL′** the degree of constraint between the Mg atom and the endocyclic oxygen atom of εCL is increased (d_{Mg-O} 2.11 *vs.* 2.23 Å). As we expected, the cleavage of the Mg–μ-OMe bond in binuclear **DTS-12CL′** requires more close contact between the methoxy oxygen atom and the carbon atom of εCL. The distance *d*[MeO–C(O)] in **DTS-12CL′** is only 1.78 Å; this distance in mononuclear **TS-12CL** is 2.04 Å. As a result, **DTS-12CL′** is characterized by a higher relative energy: 21.7 kcal mol^{-1} *vs.* 14.8 kcal mol^{-1} for **TS-12CL**.

Because **DI-2CL′** possesses an endocyclic oxygen atom coordinated to Mg, the transition to **DI-3CL′** occurs with low activation energy. Re-coordination of εCL at this stage leads to the intermediate **DI-3CL**, the energy of which is 0.7 kcal mol^{-1} lower than that of **DI-3CL′**. Transition states of the ring opening for particles containing one (**DTS-34CL′**) and two (**DTS-34CL**) molecules of εCL are similar in energy. The product of ring opening **DI-4CL** is more stable, and the additional coordination of εCL is accompanied by the dissociation of the Mg···O=C(OR) bond and leads to **DI-5CL**.

Comparison of mononuclear and binuclear mechanisms. The difference in the energies of **I-1CL** and **DI-1CL** as $\Delta G = G^{\circ}_{298}(\mathbf{I-1CL}) - 1/2G^{\circ}_{298}(\mathbf{DI-1CL}) - G^{\circ}_{298}(\varepsilon\mathrm{CL})$ is equal

to 15.7 kcal mol^{-1}. For the mononuclear mechanism, the activation energy taking **I-1CL** as the stationary point is equal to 14.8 kcal mol^{-1}. For the "pure" binuclear mechanism the activation barrier through **DTS-12CL′** taking **DI-1CL** as the starting stationary point is equal to 21.7 kcal mol^{-1}. ROP starting from **DI-1CL** and going through mononuclear **TS-12CL** is much less favorable (the activation barrier is equal to 30.5 kcal mol^{-1}). Therefore, we can conclude that lactone polymerization initiated by the dimeric magnesium complex **3** should proceed *via* the binuclear mechanism. However, when we generate the monomeric catalyst species of the type **I-1CL**, for example, by alcoholysis of monomeric complexes **1** or **2**, the mononuclear mechanism becomes the preferable reaction pathway (assuming that dimerization of **I-1CL** in viscous and diluted solution is relatively slow). This conclusion correlates strongly with the recently published results[53] and experiments reported in this article. While studying lactone ROP we found that the initial polymerization rate of the processes initiated by the catalyst obtained *in situ* from the monomeric complex (BHT)Mg(Bu)(THF)$_2$ is three times faster than that of the reaction catalyzed by bimetallic [(BHT)Mg(μ-OR)(THF)]$_2$.

Polymerization of LA

DFT modeling of lactide polymerization by "biometal" complexes performed *via* a mononuclear coordination–insertion mechanism has been discussed in tens of publications. The work[94] examines a binuclear mechanism for the initiation and propagation stages of lactide polymerization in the presence of benzyloxy Zn complex. As opposed to a several publications devoted to the mononuclear mechanism of PLA formation,[58,89,95–97] including catalysis by Mg complexes,[58,96] the paper[94] does not consider the chelate formation ability of a lactate fragment. In any case, the binuclear mechanism concept is a new idea in lactide polymerization initiated by Mg-alkoxy complexes. Here, we performed DFT calculations of reaction profiles of lactide ROP for mononuclear and binuclear mechanisms to determine which reaction pathway is preferable, and to ascertain the reasons for heterotactic polymer formation during catalysis by BHT-Mg complexes.

Mononuclear mechanism. As starting stationary points **I-1LA** we selected the adducts formed by [(DBP)Mg((*R*)-methyl lactate)GL] with (*S*,*S*)-LA or (*R*,*R*)-LA molecules. The glycolide GL, which demonstrates donor properties comparable with those of a lactide (Table 3) was taken instead of LA in **I-1LA** to simplify the calculations. The energy profile of lactide ROP *via* a monomeric mechanism is significantly more complex than that of εCL ROP. The activation barriers for nucleophilic addition of lactate to the carbonyl group of LA through **TS-1LA** are rather low, 9 kcal mol^{-1} for (*R*,*R*)-LA and 5.9 kcal mol^{-1} for (*S*,*S*)-LA. The resulting intermediate **I-2ssLA** is significantly, by 5 kcal mol^{-1}, more stable than **I-2rrLA**. The transformation from **I-2ssLA** to **I-3cssLA** through **TS-23ssLA** requires only 1.3 kcal mol^{-1} (5.6 kcal mol^{-1} relative to **I-1ssLA**), because the mutual orientation of the methyl groups of (*S*,*S*)-lactide and the coordinated (*R*)-methyl lactate in **I-2ssLA** do not hinder the formation of **I-3css**. In contrast, formation of **I-3rr** requires significant distortion of the molecular structure, and the reaction is performed *via* the high energy **TS-23rrLA** (19.3 kcal mol^{-1} relative to **I-1rrLA**). The energies of **I-3cssLA** and **I-3crrLA** are close, as are the energies of transition states **TS-33ssLA** and **TS-33rrLA** that lead to "open" tetrahedral complexes **I-3ossLA** and **I-3orrLA**. The energy of ring-opening transition state **TS-34ssLA** (17.3 kcal mol^{-1} relative to **I-1ssLA**) is higher than that of **TS-34rrLA** (15.4 kcal mol^{-1} relative to **I-1rrLA**) and is comparable in magnitude to that of **TS-23rrLA** (19.3 kcal mol^{-1} relative to **I-1rrLA**). Intermediates **I-4LA** are characterized by minimal energies of all stationary points of the reaction profiles. The stabilization of **I-4LA** is achieved through additional coordination of the oxygen atom of the ester to the Mg atom. Interaction with the LA molecule leads to intermediate **I-5LA**. Analysis of mononuclear polymerization reaction profiles of (*S*,*S*)-LA or (*R*,*R*)-LA initiated by the (*R*)-methyl lactate DBP-Mg complex (Fig. 6) gives us a difference in activation energies for enantiomeric lactides of ~2 kcal mol^{-1}. This way, the heterotactic reaction pathway is slightly more preferable.

Binuclear mechanism. Initially, we thought that we should choose the dimeric complex {(DBP)Mg[(*R*)-methyl lactate](LA)}$_2$ as the ground state for modeling the binuclear mechanism of lactide polymerization, because it is isostructural to complex **5**. Our calculations showed that unlike **DI-1CL** in polymerization of caprolactone, the loss of one molecule of LA by this complex is energetically favorable. The difference in energy is 9 kcal mol^{-1}. Therefore, the compounds {(DBP)Mg[(*R*)-methyl lactate]}$_2$(LA), **DI-1ssLA** and **DI-1rrLA**, which contain only one coordinated molecule of (*S*,*S*)- or (*R*,*R*)-lactide, were used as the starting stationary point of the binuclear mechanism of lactide ROP, and the energy profiles we obtained are presented in Fig. 6. The energies of the transition states for nucleophilic attack of the carbonyl carbon atom **DTS-12ssLA** and **DTS-12rrLA** by lactate are 20.0 and 23.5 kcal mol^{-1}, respectively. The cooperative effect, similar to that observed for **DTS-12CL**, is absent in **DTS-12LA**. This effect appears at the stage of formation of intermediates **DI-2ssLA** and **DI-2rrLA**. In contrast to the very high activation energy of **TS-23rrLA** of the mononuclear reaction pathway, coordination of the exocyclic oxygen atom after the passage of **DTS-12ssLA** and **DTS-12rrLA** does not have an activation barrier. Transition states of ring opening **DTS-23LA** possess high energies in the binuclear reaction pathway; moreover, the difference in the free energies of **DTS-23ssLA** and **DTS-23rrLA** is significant, 8.5 kcal mol^{-1}. Intermediates **DI-3cLA**, formed as a result of ring opening, are relatively unstable and transform to **DI-4LA**, which has the same coordination motif as **I-4LA**, additional coordination of the oxygen atom of the ester. The subsequent coordination of the LA molecule leads to formation of chelate complexes **DI-5LA**, which are isostructural to **DI-1LA**. Analysis of ROP reaction profiles allows us to gauge the activation energies relative to **DI-1LA** as 20.9 kcal mol^{-1} for (*S*,*S*)-LA and 29.4 kcal mol^{-1} for (*R*,*R*)-LA.

Comparison of mononuclear and binuclear mechanisms. As with εCL ROP, the binuclear mechanism of LA polymerization is energetically favorable if the pre-catalyst is a dimeric

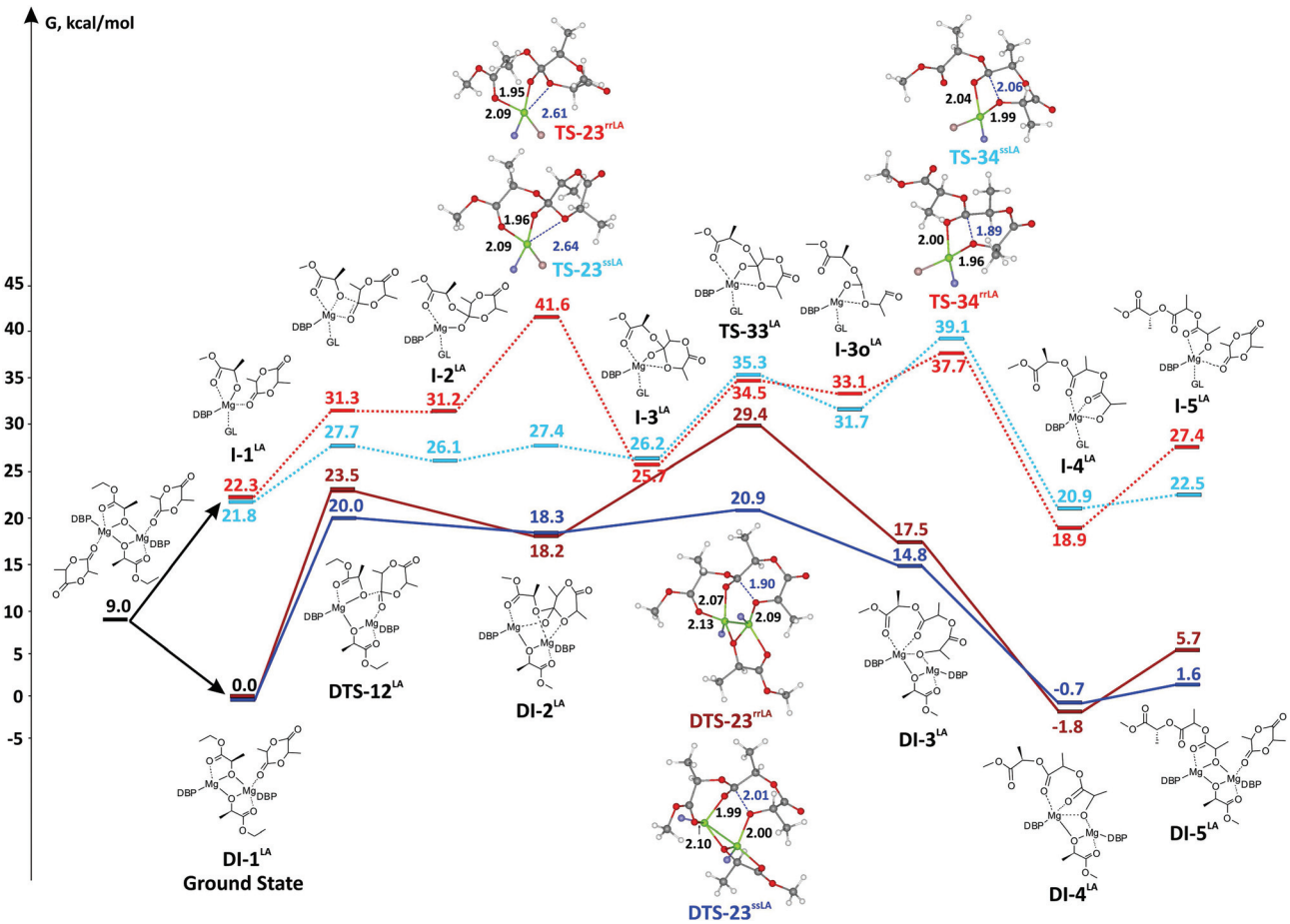

Fig. 6 Reaction profiles of lactide ROP for mononuclear and binuclear coordination–insertion mechanisms. Geometries of higher energy TS are shown; DBP and GL fragments are omitted for clarity, phenolate and GL oxygen atoms are colored in blue and pink, correspondingly.

complex such as **5**. The difference in energies between the initial stationary points **I-1ssLA/I-1rrLA** and **DI-1ssLA/DI-1rrLA** is ~22 kcal mol^{-1}. The activation energy for the mononuclear pathway of (*S*,*S*)-LA polymerization is 17.3 kcal mol^{-1} relative to mononuclear ground state **I-1LA**, whereas performing the reaction *via* the binuclear mechanism requires overcoming an activation energy of 20.9 kcal mol^{-1}. Therefore, the energetic preference for mononuclear catalytic particles is not as significant as it is in lactone polymerization (3.6 *vs.* 6.8 kcal mol^{-1}). Earlier, while performing kinetic experiments, we did not observe any difference in lactide polymerization rate between the reaction initiated by a dimeric complex and the one initiated by "monomeric" catalyst prepared *in situ.*[53] In this work, we did not fix significant difference between monomeric precatalyst **2** and dimeric complex **3** (Table 1, runs 4 and 5, correspondingly). We believe that a clearer experimental criterion for the reaction mechanism is the degree of heterotacticity of polymer P_r. In our previous work, we determined that PLA obtained by polymerization of (DL)-LA at −5 °C in the presence of the dimeric complex [(BHT)Mg(μ-OEt)(THF)]$_2$ and an initiator, synthesized *via* reaction of **2** with ethanol, were characterized by P_r values of 0.87 and 0.78, respectively.[53] The observed difference in heterotacticity confirms our calculations, according to which lactide ROP performed *via* the binuclear mechanism should lead to the formation of a polymer product with a higher degree of heterotacticity.

In conclusion, we note that catalytic systems based on BHT-magnesium complexes studied by us[53] and other colleagues,[49–52] regardless of the "living" nature of the polymerization, leads to formation of polymers with a relatively high $Đ_M$ – ~1.2–1.5. The deviation of $Đ_M$ from theoretical values of ~1.0 for living coordination polymerization is usually explained by transesterification. We propose that for BHT-Mg complexes, broadening of the molecular weight distribution can be explained by the fact that the real catalyst can be a mixture of monomeric and dimeric particles. Moreover, molecules of cyclic esters and donor solvent can take part in formation of both types of catalytic particles. When modeling εCL polymerization *via* the binuclear mechanism we determined the similarity of energy profiles for processes with catalytic particles of different amounts of coordinated substrate molecules. This leads to the diversification of the catalytic system; formation of single-type but different catalytic particles with similar but not the same geometry and energy.

Conclusion

We synthesized a series of heteroleptic BHT-Mg-OR complexes containing various types of alkoxide ligands (RO) and studied their molecular structure by X-ray diffraction. We found that complexes prepared from a primary alcohol ([(BHT)Mg(μ-OBn)(THF)]$_2$ (**3**), {(BHT)Mg[μ-O(CH$_2$)$_3$CON(CH$_3$)$_2$]}$_2$ (**7**)), from an unhindered phenol ([(BHT)Mg(μ-O-*tert*-BuC$_6$H$_4$)(THF)]$_2$ (**4**)), as well as from esters of glycolic ([(BHT)Mg(μ-OCH$_2$COOEt)(THF)]$_2$ (**5**)) and lactic ([(BHT)Mg(μ-OCH(CH$_3$)COOCH$_2$COO^{t}Bu)(THF)]$_2$ (**6**)) acids all have dimeric structures, with a Mg-(μ-OR)$_2$-Mg core. Surprisingly, the BHT-Mg-derivatives of glicolate and lactate have pentacoordinated magnesium whereas the CN_{Mg} in other BHT-Mg alcoholates is equal to 4. It has been experimentally determined that **3** and **5** are highly active catalysts of LA polymerization.

Using DOSY NMR we determined that **3** and **5** retain their dimeric structure even in a solvating solvent (THF). DFT-calculations of free energies of model dimeric [(DBP)Mg(μ-OMe)(Sub)]$_2$ and monomeric (DBP)Mg(OMe)(Sub)$_2$ complexes for a wide spectrum of solvating solvents and substrates (Sub) has shown that THF substitution with Sub in a dimeric complex is a feasible process, whereas dimer dissociation by treatment of Sub is energetically unfavorable, with an energy loss of 8–18 kcal mol_{Mg}^{-1} depending on the solvent.

We performed a comparative DFT modeling of ε-CL and (DL)-lactide ROP catalyzed by dimeric and monomeric BHT-Mg catalysts. We concluded that the binuclear mechanism is more favorable for both lactones and lactides in the initial stages of reactions catalyzed by dimeric complexes **3** and **5**.

Conflicts of interest

There are no conflicts to declare.

Acknowledgements

Financial support by the Russian Science Foundation (Grant No. 16-13-10344) is gratefully acknowledged. The NMR DOSY measurements were made at the Shared Facility Centers of the Institute of Physical Chemistry and Electrochemistry, RAS, and Institute of General and Inorganic Chemistry, RAS.

Notes and references

1 H. Tian, Z. Tang, X. Zhuang, X. Chen and X. Jing, *Prog. Polym. Sci.*, 2012, **37**, 237–280.
2 R. T. Martin, L. P. Camargo and S. A. Miller, *Green Chem.*, 2014, **16**, 1768–1773.
3 J. N. Hoskins and S. M. Grayson, *Polym. Chem.*, 2011, **2**, 289–299.
4 R. P. Brannigan and A. P. Dove, *Biomater. Sci.*, 2017, **5**, 9–21.
5 N. G. Ricapito, C. Ghobril, H. Zhang, M. W. Grinstaff and D. Putnam, *Chem. Rev.*, 2016, **116**, 2664–2704.
6 K. Fukushima, *Biomater. Sci.*, 2016, **4**, 9–24.
7 A. Gandini and T. M. Lacerda, *Prog. Polym. Sci.*, 2015, **48**, 1–39.
8 R. Klein and F. R. Wurm, *Macromol. Rapid Commun.*, 2015, **36**, 1147–1165.
9 J. Rydz, W. Sikorska, M. Kyulavska and D. Christova, *Int. J. Mol. Sci.*, 2015, **16**, 564–596.
10 Y. Zhu, C. Romain and C. K. Williams, *Nature*, 2016, **540**, 354–362.
11 G.-Q. Chen and M. K. Patel, *Chem. Rev.*, 2012, **112**, 2082–2099.
12 S. S. Bari, A. Chattarjee and S. Mishra, *Polym. Rev.*, 2016, **56**, 287–328.
13 J.-W. Rhim, H.-M. Park and C.-S. Ha, *Prog. Polym. Sci.*, 2013, **38**, 1629–1652.
14 B. D. Ulery, L. S. Nair and C. T. Laurencin, *J. Polym. Sci., Part B: Polym. Phys.*, 2011, **49**, 832–864.
15 H. R. Lakkireddy and D. Bazile, *Adv. Drug Delivery Rev.*, 2016, **107**, 289–332.
16 Z. Sheikh, S. Najeeb, Z. Khurshid, V. Verma, H. Rashid and M. Glogauer, *Materials*, 2015, **8**, 5744–5794.
17 M. Guvendiren, J. Molde, R. M. D. Soares and J. Kohn, *ACS Biomater. Sci. Eng.*, 2016, **2**, 1679–1693.
18 A. J. T. Teo, A. Mishra, I. Park, Y.-J. Kim, W.-T. Park and Y.-J. Yoon, *ACS Biomater. Sci. Eng.*, 2016, **2**, 454–472.
19 S. Farah, D. G. Anderson and R. Langer, *Adv. Drug Delivery Rev.*, 2016, **107**, 367–392.
20 E. Castro-Aguirre, F. Iñiguez-Franco, H. Samsudin, X. Fang and R. Auras, *Adv. Drug Delivery Rev.*, 2016, **107**, 333–366.
21 M. Santoro, S. R. Shah, J. L. Walker and A. G. Mikos, *Adv. Drug Delivery Rev.*, 2016, **107**, 206–212.
22 E. A. Rainbolt, K. E. Washington, M. C. Biewer and M. C. Stefan, *Polym. Chem.*, 2015, **6**, 2369–2381.
23 J.-M. Raquez, Y. Habibi, M. Murariu and P. Dubois, *Prog. Polym. Sci.*, 2013, **38**, 1504–1542.
24 G. Narayanan, V. N. Vernekar, E. L. Kuyinu and C. T. Laurencin, *Adv. Drug Delivery Rev.*, 2016, **107**, 247–276.
25 A.-C. Albertsson and I. K. Varma, *Biomacromolecules*, 2003, **4**, 1466–1486.
26 S. Ruengdechawiwat, R. Somsunan, R. Molloy, J. Siripitayananon, V. J. Franklin, P. D. Topham and B. J. Tighe, *Adv. Mater. Res.*, 2014, **894**, 172–176.
27 L. Wang, V. Poirier, F. Ghiotto, M. Bochmann, R. D. Cannon, J.-F. Carpentier and Y. Sarazin, *Macromolecules*, 2014, **47**, 2574–2584.
28 J.-M. Raquez, R. Mincheva, O. Coulembier and P. Dubois, in *Polymer Science: A Comprehensive Reference*, ed. K. Matyjaszewski and M. Möller, 2012, vol. 4, pp. 761–778.
29 R. H. Platel, L. M. Hodgson and C. K. Williams, *Polym. Rev.*, 2008, **48**, 11–63.
30 C. A. Wheaton, P. G. Hayes and B. J. Ireland, *Dalton Trans.*, 2009, 4832–4846.
31 C. M. Thomas, *Chem. Soc. Rev.*, 2010, **39**, 165–173.
32 M. J. Stanford and A. P. Dove, *Chem. Soc. Rev.*, 2010, **39**, 486–494.
33 R. Jianming, X. Anguo, W. Hongwei and Y. Hailin, *Des. Monomers Polym.*, 2014, **17**, 345–355.

34 B. Calvo, M. G. Davidson and D. García-Vivó, *Inorg. Chem.*, 2011, **50**, 3589–3595.
35 W. Yi and H. Ma, *Inorg. Chem.*, 2013, **52**, 11821–11835.
36 J. Zhang, J. Xiong, Y. Sun, N. Tang and J. Wu, *Macromolecules*, 2014, **47**, 7789–7796.
37 A. Duda and A. Kowalski, in *Handbook of ring-opening polymerization*, ed. P. Dubois, O. Coulembier and J.-M. Raquez, 2009, pp. 1–52.
38 L. Wang and H. Ma, *Macromolecules*, 2010, **43**, 6535–6537.
39 S. Song, H. Ma and Y. Yang, *Dalton Trans.*, 2013, **42**, 14200–14211.
40 J.-C. Wu, B.-H. Huang, M.-L. Hsueh, S.-L. Lai and C.-C. Lin, *Polymer*, 2005, **46**, 9784–9792.
41 Y. Gao, Z. Dai, J. Zhang, X. Ma, N. Tang and J. Wu, *Inorg. Chem.*, 2014, **53**, 716–726.
42 Y. Wang, W. Zhao, X. Liu, D. Cui and E. Y.-X. Chen, *Macromolecules*, 2012, **45**, 6957–6965.
43 H.-J. Chuang, H.-L. Chen, J.-L. Ye, Z.-Y. Chen, P.-L. Huang, T.-T. Liao, T.-E. Tsai and C.-C. Lin, *J. Polym. Sci., Part A: Polym. Chem.*, 2013, **51**, 696–707.
44 C.-Y. Sung, C.-Y. Li, J.-K. Su, T.-Y. Chen, C.-H. Lin and B.-T. Ko, *Dalton Trans.*, 2012, **41**, 953–961.
45 J. Ejfler, K. Krauzy-Dziedzic, S. Szafert, L. B. Jerzykiewicz and P. Sobota, *Eur. J. Inorg. Chem.*, 2010, 3602–3609.
46 M. H. Chisholm, J. Gallucci and K. Phomphrai, *Inorg. Chem.*, 2002, **41**, 2785–2794.
47 P. Brignou, S. M. Guillaume, T. Roisnel, D. Bourissou and J.-F. Carpentier, *Chem. – Eur. J.*, 2012, **18**, 9360–9370.
48 J. Calabrese, M. A. Cushing Jr. and S. D. Ittel, *Inorg. Chem.*, 1988, **27**, 867–870.
49 H.-Y. Chen, L. Mialon, K. A. Abboud and S. A. Miller, *Organometallics*, 2012, **31**, 5252–5261.
50 H.-J. Fang, P.-S. Lai, J.-Y. Chen, S. C. N. Hsu, W.-D. Peng, S.-W. Ou, Y.-C. Lai, Y.-J. Chen, H. Chung, Y. Chen, T.-C. Huang, B.-S. Wu and H.-Y. Chen, *J. Polym. Sci., Part A: Polym. Chem.*, 2012, **50**, 2697–2704.
51 J. A. Wilson, S. A. Hopkins, P. M. Wright and A. P. Dove, *Polym. Chem.*, 2014, **5**, 2691–2694.
52 J. A. Wilson, S. A. Hopkins, P. M. Wright and A. P. Dove, *Macromolecules*, 2015, **48**, 950–958.
53 I. E. Nifant'ev, A. V. Shlyakhtin, A. N. Tavtorkin, P. V. Ivchenko, R. S. Borisov and A. V. Churakov, *Catal. Commun.*, 2016, **87**, 106–111.
54 J. D. Monegan and S. D. Bunge, *Inorg. Chem.*, 2009, **48**, 3248–3256.
55 K. W. Henderson, G. W. Honeyman, A. R. Kennedy, R. E. Mulvey, J. A. Parkinson and D. C. Sherrington, *Dalton Trans.*, 2003, 1365–1372.
56 C. R. Groom and F. H. Allen, *Angew. Chem., Int. Ed.*, 2014, **53**, 662–671.
57 C. R. Groom, I. J. Bruno, M. P. Lightfoot and S. C. Ward, *Acta Crystallogr., Sect. B: Struct. Sci.*, 2016, **72**, 171–179.
58 E. L. Marshall, V. C. Gibson and H. S. Rzepa, *J. Am. Chem. Soc.*, 2005, **127**, 6048–6051.
59 J. Lewiński, J. Zachara and I. Justyniak, *Chem. Commun.*, 1997, 1519–1520.
60 J. Lewiński, J. Zachara and I. Justyniak, *Organometallics*, 1997, **16**, 4597–4605.
61 J. Lewiński, P. Horeglad, K. Wójcik and I. Justyniak, *Organometallics*, 2005, **24**, 4588–4593.
62 N. Nomura, R. Ishii, Y. Yamamoto and T. Kondo, *Chem. – Eur. J.*, 2007, **13**, 4433–4451.
63 K. Phomphrai, P. Chumsaeng, P. Sangtrirutnugul, P. Kongsaeree and M. Pohmakotr, *Dalton Trans.*, 2010, **39**, 1865–1871.
64 S. Dagorne, F. Le Bideau, R. Welter, S. Bellemin-Laponnaz and A. Maisse-François, *Chem. – Eur. J.*, 2007, **13**, 3202–3217.
65 V. Balasanthiran, M. H. Chisholm, K. Choojun and C. B. Durr, *Dalton Trans.*, 2014, **43**, 2781–2788.
66 P. Horeglad, P. Kruk and J. Pécaut, *Organometallics*, 2010, **29**, 3729–3734.
67 J. S. Klitzke, T. Roisnel, E. Kirillov, O. de L. Casagrande Jr. and J.-F. Carpentier, *Organometallics*, 2014, **33**, 309–321.
68 H. Wang, Y. Yang and H. Ma, *Macromolecules*, 2014, **47**, 7750–7764.
69 V. Gutmann, *Coord. Chem. Rev.*, 1976, **18**, 225–255.
70 S. Ghosh, P. K. S. Antharjanam and D. Chakraborty, *Polymer*, 2015, **70**, 38–51.
71 O. Dechy-Cabaret, B. Martin-Vaca and D. Bourissou, *Chem. Rev.*, 2004, **104**, 6147–6176.
72 P. Degée, P. Dubois, R. Jerôme, S. Jacobsen and H.-G. Fritz, *Macromol. Symp.*, 1999, **144**, 289.
73 A. Macchioni, G. Ciancaleoni, C. Zuccaccia and D. Zuccaccia, *Chem. Soc. Rev.*, 2008, **37**, 479–489.
74 A. Einstein, *Investigations on the Theory of the Brownian Movement*, Dover Publications Inc., Mineola, NY, 1956.
75 D. Li, G. Kagan, R. Hopson and P. G. Williard, *J. Am. Chem. Soc.*, 2009, **131**, 5627–5634.
76 G. Kagan, W. Li, R. Hopson and P. G. Williard, *Org. Lett.*, 2009, **11**, 4818–4821.
77 B. M. Schulze, D. L. Watkins, J. Zhang, I. Ghiviriga and R. K. Castellano, *Org. Biomol. Chem.*, 2014, **12**, 7932–7936.
78 D. Jędrzkiewicz, J. Ejfler, N. Gulia, Ł. John and S. Szafert, *Dalton Trans.*, 2015, **44**, 13700–13715.
79 A. Gierer and K. Wirtz, *Z. Naturforsch., A: Astrophys. Phys. Phys. Chem.*, 1953, **8**, 532–538.
80 H. C. Chen and S. H. Chen, *J. Phys. Chem.*, 1984, **88**, 5118–5121.
81 F. Cataldo, *Eur. Chem. Bull.*, 2015, **4**, 92–97.
82 M. Kuzdrowska, L. Annunziata, S. Marks, M. Schmid, C. G. Jaffredo, P. W. Roesky, S. M. Guillaume and L. Maron, *Dalton Trans.*, 2013, **42**, 9352–9360.
83 E. E. Marlier, J. A. Macaranas, D. J. Marell, C. R. Dunbar, M. A. Johnson, Y. DePorre, M. O. Miranda, B. D. Neisen, C. J. Cramer, M. A. Hillmyer and W. B. Tolman, *ACS Catal.*, 2016, **6**, 1215–1224.
84 K. Ding, M. O. Miranda, B. Moscato-Goodpaster, N. Ajellal, L. E. Breyfogle, E. D. Hermes, C. P. Schaller, S. E. Roe, C. J. Cramer, M. A. Hillmyer and W. B. Tolman, *Macromolecules*, 2012, **45**, 5387–5396.

85 M.-C. Chang, W.-Y. Lu, H.-Y. Chang, Y.-C. Lai, M. Y. Chiang, H.-Y. Chen and H.-Y. Chen, *Inorg. Chem.*, 2015, **54**, 11292–11298.
86 M. O. Miranda, Y. DePorre, H. Vazquez-Lima, M. A. Johnson, D. J. Marell, C. J. Cramer and W. B. Tolman, *Inorg. Chem.*, 2013, **52**, 13692–13701.
87 J. Jitonnom, R. Molloy, W. Punyodom and W. Meelua, *Comput. Theor. Chem.*, 2016, **1097**, 25–32.
88 J. Wei, M. N. Riffel and P. L. Diaconescu, *Macromolecules*, 2017, **50**, 1847–1861.
89 S. Vogt-Geisse, R. A. Matac and A. Toro-Labbé, *Phys. Chem. Chem. Phys.*, 2017, **19**, 8989–8999.
90 I. E. Nifant'ev, P. V. Ivchenko, A. V. Shlyakhtin and A. V. Ivanyuk, *Polym. Sci., Ser. B*, 2017, **59**, 147–156.
91 I. del Rosal, P. Brignou, S. M. Guillaume, J.-F. Carpentier and L. Maron, *Polym. Chem.*, 2015, **6**, 3336–3352.
92 I. del Rosal, P. Brignou, S. M. Guillaume, J.-F. Carpentier and L. Maron, *Polym. Chem.*, 2011, **2**, 2564–2573.
93 C. Sattayanon, W. Sontising, W. Limwanich, P. Meepowpan, W. Punyodom and N. Kungwan, *Struct. Chem.*, 2015, **26**, 695–703.
94 C. Fliedel, D. Vila-Viçosa, M. J. Calhorda, S. Dagorne and T. Avilés, *ChemCatChem*, 2014, **6**, 1357–1367.
95 S. Tabthong, T. Nanok, P. Sumrit, P. Kongsaeree, S. Prabpai, P. Chuawong and P. Hormnirun, *Macromolecules*, 2015, **48**, 6846–6861.
96 P. V. Ivchenko, A. V. Shlyakhtin and I. E. Nifant'ev, *Mendeleev Commun.*, 2017, **27**, 278–280.
97 C. Robert, T. E. Schmid, V. Richard, P. Haquette, S. K. Raman, M.-N. Rager, R. M. Gauvin, Y. Morin, X. Trivelli, V. Guérineau, I. del Rosal, L. Maron and C. M. Thomas, *J. Am. Chem. Soc.*, 2017, **139**, 6217–6225.